Prepulse suppression and optimization of backward Raman amplification with a chirped pump laser beam

R. Nuter and V. Tikhonchuk

Université Bordeaux-CNRS-CEA, Centre Lasers Intenses et Applications, UMR No. 5107, F-33405 Talence, France

(Received 26 February 2013; published 22 April 2013)

Two-dimensional particle-in-cell (PIC) simulations have been performed to demonstrate how chirping the pump laser beam can make the seed backward Raman amplification more efficient. The PIC code OCEAN is detailed and validated with theoretical analysis of the three-wave coupling. Particular attention is devoted to the impact of numerical noise on Raman scattering. Once the numerical parameters are set, one- and two-dimensional simulations exhibit the ability to suppress the pedestal pulse preceding the amplified seed laser beam and lower the spontaneous Raman scattering by appropriately choosing the pump chirp value.

DOI: 10.1103/PhysRevE.87.043109 PACS number(s): 52.38.Bv, 42.65.Dr, 52.65.Rr

I. INTRODUCTION

The backward Raman amplification has attracted much interest as a candidate for the challenging development of the next generation of high-power laser systems [1]. It consists in amplifying and compressing in a plasma a Stokes-shifted laser pulse (seed pulse) by counterpropagating a long duration and a relatively-low-power laser beam (pump pulse) [2,3]. Using a plasma as a gain medium may allow one to achieve, without irreparable damages, higher intensities than those usually reached with the chirped pulse amplification technique in solids or liquids. This innovative amplification technique has already demonstrated its ability to produce high laser intensities [3–5], but with a low efficiency of the pump to seed energy transfer. It is essential to find the physical setup able to optimize the process of backward Raman amplification and to control the pulse quality.

The energy transfer rate from the pump laser beam to the seed one is governed by the Langmuir plasma wave. The higher the plasma wave amplitude, the stronger the three-wave coupling rate and the more efficient the pump to seed energy transfer. Excitation of the plasma wave is limited by the wavebreaking process, which occurs as the electrons, accelerated via the electrostatic field, reach a velocity close to the phase velocity of the electrostatic wave. By perturbing the collective motion of plasma electrons, the wavebreaking makes the three-wave coupling less efficient. Therefore, the stimulated Raman scattering of the pump beam from the spontaneous noise has to be controlled so that it does not break the plasma before the interaction between the pump and the seed beams.

Some solutions have been proposed to enhance the backward Raman amplification of the seed pulse and to suppress the spontaneous Raman signal. Malkin *et al.* [6] have proposed the use of a plasma with a longitudinal density gradient to detune the phase mismatch between the pump beam, the spontaneous scattering wave, and the Langmuir wave, avoiding an amplification of the parasitic spontaneous Raman signal. Ersfeld and Jaroszynski [7] have suggested that this detuning be created by chirping the pump laser pulse. Both studies have been conducted in the one-dimensional (1D) geometry disregarding two-dimensional effects. Moreover, their analysis was restricted to circularly polarized laser beams known to reduce the electron plasma heating because of the absence of the time oscillating ponderomotive force. Vieux *et al.* [8] have experimentally studied the effect of pump chirping on Raman amplification, but without looking for an optimization of the Raman amplification. Chirping the pump laser beam to optimize the backward Raman amplification has already been suggested by Caird [9]; however, this study was conducted with a gas cell instead of a plasma as a gain medium.

Recent two- and three-dimensional simulations [10,11] have demonstrated favorable parameters for backward Raman amplification in a low-density plasma. However, the role of spontaneous Raman scattering amplification was not discussed, nor was the role of plasma heating and detuning. These issues are important for controlling the amplified pulse shape and the prepulse.

In this paper we show how chirping the pump laser beam can reduce the spontaneous Raman scattering and increase in the same way the Raman amplification of the seed laser beam. We briefly recall the linear and nonlinear regimes of the Raman scattering. The PIC code OCEAN is described and applied to the analytical results. Numerical simulations performed in 1D and 2D geometries show how chirping the pump laser beam is able to optimize the backward Raman amplification.

II. THEORETICAL ANALYSIS

The backward Raman scattering occurs when an incident pump laser beam, with the frequency ω_0 and the wave vector $\vec{k}_0$, decays into a plasma wave ($\omega_{p,e}$, $\vec{k}_{p,e}$) and a backscattered electromagnetic beam ($\omega_s = \omega_0 - \omega_{p,e}, \vec{k}_s = \vec{k}_0 - \vec{k}_{p,e}$), where $\omega_{p,e} \approx \omega_{p,0} = \sqrt{n_0 e^2/m_e\epsilon_0}$ is the plasma frequency, n_0 is the plasma density, e and m_e are the electron charge and mass, respectively, and ϵ_0 is the dielectric permittivity of vacuum. Neglecting the diffraction effects, the temporal and spatial dynamics of these waves are described with the following system of three dimensionless equations [2]:

$$\begin{aligned}\left[\frac{\partial}{\partial t} + v_{g,p}\frac{\partial}{\partial x}\right] a_p &= -\Gamma a_e a_s,\\ \left[\frac{\partial}{\partial t} - v_{g,s}\frac{\partial}{\partial x}\right] a_s &= \Gamma a_e a_p,\\ \left[\frac{\partial}{\partial t} + v_{g,e}\frac{\partial}{\partial x}\right] a_e &= \Gamma a_p a_s,\end{aligned} \tag{1}$$

where t and x are normalized to $1/\omega_0$ and c/ω_0, respectively. The amplitudes of the pump, the seed beams, and the Langmuir plasma wave are $a_p = 0.85\sqrt{I_p\lambda_0^2}$ (where I_p is the pump laser intensity expressed in units of 10^{18} W/cm^2 and λ_0 is the pump wavelength expressed in microns), $a_s = 0.85\sqrt{\omega_0/\omega_s}\sqrt{I_s\lambda_0^2}$ (where I_s is the seed laser intensity expressed in units of 10^{18} W/cm^2), and $a_e = \sqrt{\omega_0/\omega_{p,e}}E/E_c$ (where $E_c = m_e\omega_0 c/e$ is the Compton field amplitude and E is the plasma electrostatic field), respectively. The three-wave coupling factor, normalized to ω_0, is $\Gamma = \frac{1}{4}\frac{k_{p,e}c}{\omega_0}\sqrt{\frac{\omega_{p,e}}{\omega_s}}$. The group velocities of the scattered and pump beams, normalized to c (the light velocity in vacuum), are $v_{g,s} = k_s c/\omega_s$ and $v_{g,p} = k_p c/\omega_p$, respectively, and $v_{g,e} = 3k_{p,e}v_{te}^2/\omega_{pe}c$, with v_{te} the electron thermal velocity. The plasma wave velocity is small and for all practical conditions it can be neglected, so $v_{g,e} = 0$ in what follows. These equations model also the backward Raman amplification process when the scattered beam is injected from the plasma's right-hand side boundary limit.

In the linear regime, the pump wave is assumed to not be depleted by the Raman scattering so that its amplitude is kept constant. The previous equations are then reduced to

$$\left[\frac{\partial}{\partial t} - v_{g,s}\frac{\partial}{\partial x}\right]a_s = \Gamma_0 a_e, \quad \frac{\partial}{\partial t}a_e = \Gamma_0 a_s, \tag{2}$$

where $\Gamma_0 = \Gamma a_p \simeq \frac{1}{2}a_p(n_0/n_c)^{1/4}$ is the backward Raman growth rate normalized to ω_0 with $n_c = m_e\epsilon_0\omega_p^2/e^2$ the plasma critical density for the laser pump. The solution of Eqs. (2) reads

$$a_s(x,t) = a_{s,0}I_0\left[\frac{2\Gamma_0}{v_{g,s}}\sqrt{(L-x)v_{g,s}(t-t^*)-(L-x)^2}\right], \tag{3}$$

where $I_0(x)$ is the modified Bessel function of the first kind, L is the plasma length, and t^* is the time at which the seed laser beam with the initial amplitude $a_{s,0}$ is injected at $x = L$. It is supposed that t^* corresponds to the time at which the pump laser beam reaches the right end of the plasma, so that $t^* \sim L/v_{g,p}$.

When the Raman amplification is so strong that it contributes to the depletion of the pump laser energy, the seed laser amplitude is modeled with the system of equations (1), where the plasma wave velocity $v_{g,e}$ is neglected. By setting $X = L - x$ and $\tau = t - \frac{L-x}{v_{g,s}}$, we obtain

$$\begin{aligned}\left[1+\frac{v_{g,p}}{v_{g,s}}\right]\frac{\partial a_p}{\partial \tau} - v_{g,p}\frac{\partial a_p}{\partial X} &= -\Gamma a_e a_s,\\ v_{g,s}\frac{\partial a_s}{\partial X} &= \Gamma a_e a_p,\\ \frac{\partial a_e}{\partial \tau} &= \Gamma a_p a_s.\end{aligned} \tag{4}$$

The nonlinear stage occurs when the pump depletion becomes noticeable. In this case, the amplitude of the seed laser beam increases and its duration decreases with time. The distance between the seed maximum and the pump pulse front is also decreasing such that $\Delta a_p/\Delta\tau \gg v_{g,p}\,\Delta a_p/\Delta X$. The spatial derivative term can then be neglected so that the first and third equations (4) result in

$$\frac{1}{1+\frac{v_{g,p}}{v_{g,s}}}\frac{\partial a_e^2}{\partial \tau} + \frac{\partial a_p^2}{\partial \tau} = 0, \tag{5}$$

$$a_s = \frac{1}{\Gamma a_p}\frac{\partial a_e}{\partial \tau}. \tag{6}$$

Thus, according to (5) and (6), one can represent the solutions in the form

$$a_p = a_0\cos(u/2), \tag{7}$$

$$a_e = \sqrt{1+\frac{v_{g,p}}{v_{g,s}}}a_0\sin(u/2), \tag{8}$$

$$a_s = \frac{1}{2\Gamma}\sqrt{1+\frac{v_{g,p}}{v_{g,s}}}\frac{\partial u}{\partial \tau}, \tag{9}$$

where u verifies the sine-Gordon equation

$$v_{g,s}\frac{\partial^2 u}{\partial X\partial\tau} = \Gamma^2 a_0^2\sin u. \tag{10}$$

The general solution of this equation is unknown [12]. However, a variety of particular solutions have been discovered. The signal amplification is described by the π-pulse solution [2,13]. By setting $z = \frac{2\Gamma a_0}{\sqrt{v_{g,s}}}\sqrt{X\tau}$, the sine-Gordon equation reduces to

$$\frac{\partial^2 u}{\partial z^2} + \frac{1}{z}\frac{\partial u}{\partial z} = \sin u. \tag{11}$$

A numerical solution is presented in Fig. 1 by the black solid curve, where the initial conditions are $u(z \to 0) = \epsilon_0 = 0.1$ and $\partial u/\partial z(z \to 0) = 0$.

Malkin *et al.* [2] have suggested that for $\epsilon_0 < 1$, the solution of the sine-Gordon equation can be approximated with the expression $u(z) = 4\tan^{-1}(\epsilon_0 e^z/4\sqrt{2\pi z})$. The seed intensity computed from the z derivative of this analytical expression is displayed in Fig. 1 by the blue dashed curve. It exhibits relatively good agreement with the first peak of the numerical solution.

The amplitude of the seed pulse increases proportionally to the plasma length while the pulse width decreases inversely proportionally to the distance. This is the so-called π-pulse solution [2].

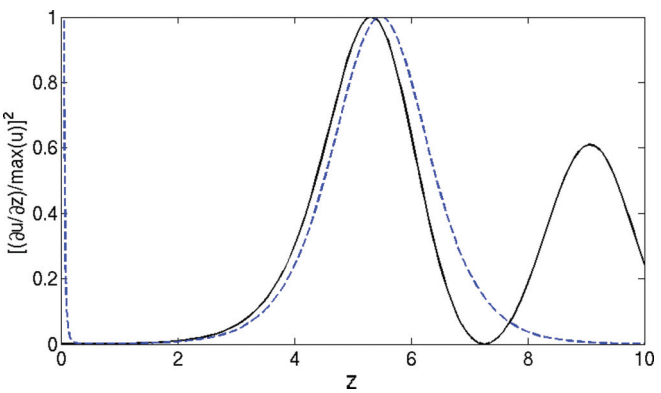

FIG. 1. (Color online) Normalized seed intensity $[\frac{\partial u}{\partial z}/\max(u)]^2$ obtained from numerical integration (black solid curve) and the approximated solution (blue dashed curve) of Eq. (11).

In the limit of strong pump depletion, which is of main interest for the Raman amplification, $\Gamma a_0 L/v_{g,s} \gg 1$, this solution describes approximatively a linear increase of the seed intensity with the coordinate. This can be explained qualitatively as follows. The pump wave energy is fully transferred to the probe laser beam so that the number of photons lost by the pump laser beam $\Delta N_p = \frac{I_p}{\hbar\omega_p}\frac{v_{g,s}}{v_{g,p}}\Delta t$ over the interval $\Delta t = \Delta X/v_{g,s}$ is equal to the number of photons gained by the seed wave $\Delta N_s = \frac{\Delta I_s}{\hbar\omega_s}\tau_s$ (τ_s is the pulse duration of the seed). This full energy transfer results in an amplification factor equal to $\Delta I_s/\Delta t \simeq I_p/\tau_s$.

III. NUMERICAL TOOLS

The numerical simulations have been performed with the PIC code OCEAN, which models the laser-plasma interaction in 1D and 2D geometries by simultaneously solving the Maxwell equations and the Vlasov equation for each charge species [14]. As for the PIC code PICLS [15], the Maxwell-Ampère and Maxwell-Faraday equations are solved with the directional splitting method, which consists in successively solving these equations along each direction. This numerical method presents the advantages of being dispersionless along the pump propagation axis and stable with a relatively large time step $\Delta t = c\Delta x$, where Δx is the mesh size. The macroparticles dynamics is relativistic and is computed with the Boris pusher [14]. The current densities, source terms of the Maxwell-Ampère equation, are solved according to the charge-conserving scheme developed by Esirkepov [16] with a form factor order equal to 3. The OCEAN code is parallelized over a domain decomposition. With the directional splitting technique, two-dimensional simulations verify the Maxwell-Gauss equation with an accuracy close to 0.001%.

A. Linear amplification

We compare the PIC code OCEAN results with the analytical formula [Eq. (3)] by simulating the backward Raman amplification in a one-dimensional geometry. The pump and seed laser pulses, modeled with plane waves, are characterized by $a_{p,0} = 0.05$ and $a_{s,0} = 0.0005$. The plasma is characterized by a $100\lambda_p$ length ($628.32c/\omega_0$) and is composed of protons and electrons with a temperature initially zero and a density equal to $0.03n_c$. The seed laser pulse is temporally delayed by $t^* \sim L/v_{g,p}$ so that it interacts with the plasma as the pump laser beam reaches the right-hand boundary. The mesh size has been set to $\Delta x = \lambda_p/20$. We have chosen 2000 macroparticles per mesh and the ions motion is frozen.

The solid curve in Fig. 2(a) displays the temporal evolution of the seed laser amplitude numerically computed at $x = 314.16c/\omega_0$ (middle of the plasma). As soon as the seed laser pulse reaches this position (around $\omega_0 t \approx 1000$), its amplitude increases up to $a_s/E_c = 0.026$ and then decreases. The seed amplitude value is kept lower than the pump one so that the backward Raman scattering occurs in the linear regime. We observe that the seed amplitude increase is perfectly reproduced with the analytical formula given in Eq. (3) and shown by the dashed line. The discrepancy between theoretical and numerical results occurs around $\omega_0 t \approx 1300$, with the latter displaying a saturation. It originates from the Langmuir plasma wavebreaking [17], where electrons escaped from the trapping waves suppress the Raman scattering. Neglecting the electron temperature, we can approximate the wave amplitude for which plasma breaks by $a_{e,\max} = n_e/2n_c$. Figure 2(b) shows the electrostatic field computed at $x = 314.16c/\omega_0$. We observe that the maximum wave amplitude is reached around $\omega_0 t \approx 1300$, the time at which the seed amplitude saturates. The saturation value is close to the expected value $a_{e,\max} = 0.015$.

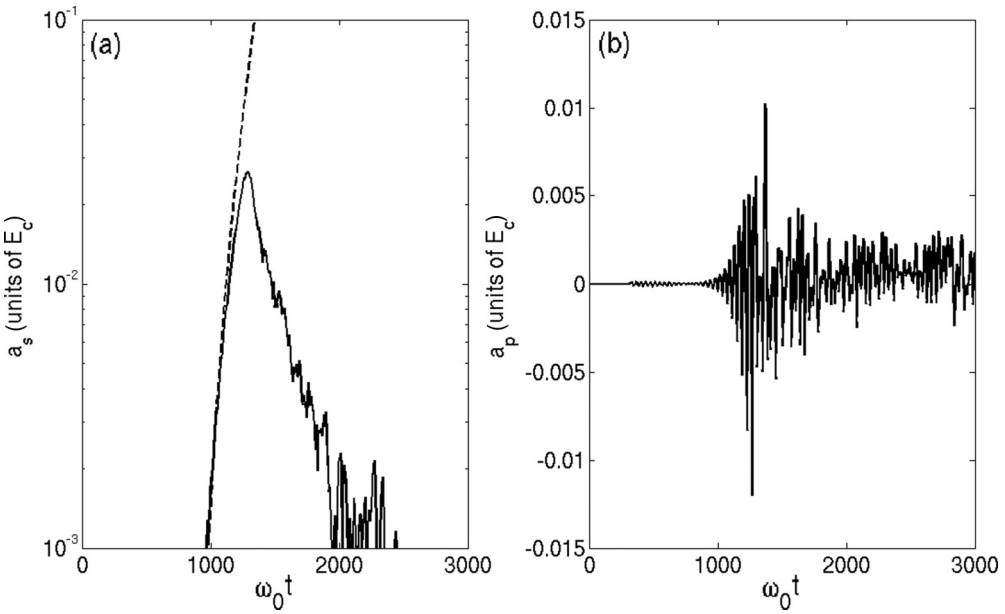

FIG. 2. Temporal evolution of (a) the seed laser amplitude and (b) the electrostatic field at the position $x = 314.16c/\omega_0$ for $n_e/n_c = 0.03$. Numerical results are displayed by solid curves and theoretical backward Raman amplification is shown by a dashed curve.

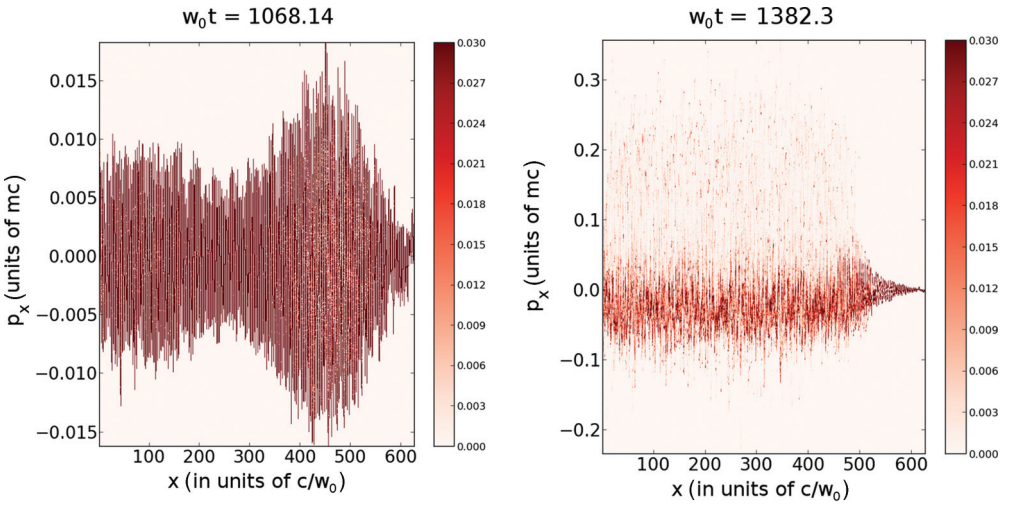

FIG. 3. (Color online) Phase space x-p_x for electrons at $\omega_0 t \approx 1100$ and 1400. Here m and c denote the electron mass and the light velocity in vacuum, respectively.

The effect of plasma wavebreaking is illustrated in Fig. 3, where the x-p_x phase space for electrons is shown before (left) and after (right) the plasma wavebreaking time. In the left panel, one can see the collective motion of electrons in the electrostatic field. This plasma oscillation is essential for the backward Raman amplification. Once electrons have reached the phase velocity of the plasma wave, they are no longer trapped in this collective oscillation and the plasma wave breaks. This leads to strong electron heating and acceleration in the forward direction, as illustrated in the right panel.

The temporal evolution of the seed laser amplitude for several plasma densities $n_e/n_c = 0.001$, 0.01, 0.02, and 0.03 is presented in Fig. 4. The analytical formula computed in the linear regime reproduces well the amplification of the seed laser beam before the plasma wave breaks. In agreement with the theory [17], the saturation amplitude of the seed beam increases as the plasma density increases. This originates from the increase of the plasma wavebreaking amplitude with the plasma density ($a_{e,\max} = n_e/2n_c$). This excellent agreement between theoretical analysis and numerical simulations validates the PIC code OCEAN.

B. Noise level evaluation

Here we analyze the influence of the numerical noise on the Raman scattering process. For this purpose, we look at the reflectivity on the left boundary of the numerical box, which corresponds to the ratio between the electromagnetic energy flux leaving the plasma over the energy flux of the pump laser entering it. The dependence of reflectivity on the number of macroparticles per cell is illustrated in Fig. 5, where the fluxes have been averaged over the pump optical period. All cases display a peak in the reflectivity for early times. It originates from the reflection of the pump laser beam on the plasma edge compression produced as the pump laser steep front enters the plasma. A modulation of the reflectivity on the plasma period ($\tau_{p,e} = 36.321/\omega_0$) corresponds to the backward Raman scattering.

Let us now focus our attention on the 1D geometry results. Increasing the number of macroparticles per cell from 10 to 500 reduces, for time shorter than $400\omega_0^{-1}$, the reflectivity by a factor 10. This enables the reflectivity to reach values close to the one computed from the Fresnel theory $r = (\frac{1-n}{1+n})^2$, with $n \approx \sqrt{1 - n_e/n_c}$ the plasma refractive index (for $n_e/n_c = 0.03$, $r = 7 \times 10^{-5}$). Over this time interval, a small part of the pump laser field is then reflected from the plasma gradient. An increase in the reflectivity for longer time results from the stimulated Raman scattering of the pump beam from the spontaneous plasma wave fluctuations. This increase is time delayed as the number of macroparticles per cell is increased from 500 to 1000. It is due to the numerical noise reduction as the number of macroparticles per cell increases. The convergence is reached for 1000 macroparticles per cell. The reflectivity is saturating around a value equal to 0.1. As explained previously, this saturation comes from the plasma wavebreaking. These 1D results clearly show that the number of macroparticles per cell has to be sufficiently high in order that the numerical noise does not enhance the pump reflection on the plasma-vacuum interface and the backward Raman scattering.

Now let us look at the 2D results displayed in Fig. 5 by black curves. The level of noise and the reflectivity are lower than those computed in a one-dimensional geometry. This originates from the spatial distribution of the pump laser beam, which is not a plane wave (as it is for 1D simulation) but a $\cos^2$ distribution.

It is important to evaluate the impact of the steepness of the pump laser front on the Raman scattering. The excitation of the Raman instabilities has to be held on a low level before the seed pulse interacts with the pump laser beam. The pump pulse with a ramp time τ is modeled with

$$a_p(t) = a_{p,0}\,\frac{t}{\tau}\,e^{i\omega_0 t} \quad \text{for} \quad 0 \leqslant t \leqslant \tau, \tag{12}$$

$$a_p(t) = a_{p,0}\,e^{i\omega_0 t} \quad \text{for} \quad t \geqslant \tau. \tag{13}$$

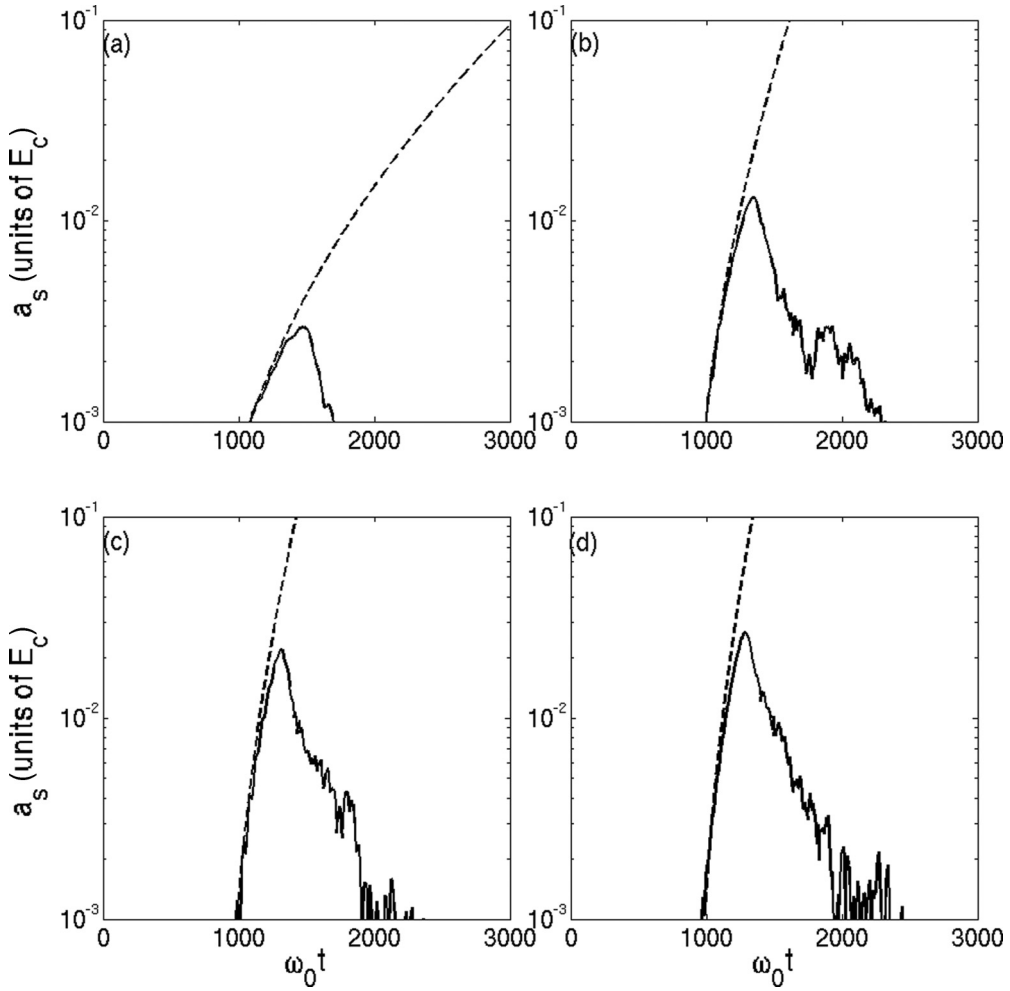

FIG. 4. Temporal evolution of the seed laser amplitude at the position $x = 314.16c/\omega_0$. Numerical results (solid curves) are compared with the analytical formula (dashed curves) from the linear regime for $n_e/n_c = 0.001$ (a), 0.01 (b), 0.02 (c), and 0.03 (d).

Its spectrum, computed from the Fourier transform of Eq. (12), is written as

$$|\tilde{a}_p(\omega)| = \frac{a_{p,0}\tau}{\sqrt{2\pi}} \frac{\sqrt{2+\theta^2-2\cos(\theta)-2\theta\sin(\theta)}}{\theta^2}, \qquad (14)$$

with $\theta = (\omega_0 - \omega)\tau$. In its drawing in Fig. 6, we observe that the full frequency bandwidth at half maximum is equal to $10/\tau$. The steeper the pump laser front, the larger the frequency bandwidth of excited waves. The Stokes wave is then notably excited if the Raman frequency ω_s belongs to the interval $[\omega_0 - 5/\tau, \omega_0]$. This leads to the following condition of suppression of the forward Raman scattering: $\tau/T_{\rm opt} > 0.8/\sqrt{n_e/n_c}$, with $T_{\rm opt}$ the pump field optical period. By evaluating the wave-number spectrum, which behaves as Eq. (14), we conclude that only the forward Raman instability is excited by the pump laser front.

Figure 7 displays the reflectivities obtained with several pump ramp times. Choosing a ramp higher than $5T_{\rm opt}$ enables the reflectivity decrease for the plasma densities higher than 1% of the critical density. This result agrees with the condition $\tau/T_{\rm opt} \geqslant 0.8/\sqrt{n_e/n_c}$. The decrease of excitation of Raman instabilities with the ramp time increase is confirmed by the bottom panel of Fig. 7, displaying the spectral dependence of the electrostatic fields. Both forward ($|k_{p,e}| = 0.177\ \omega_0/c$) and backward ($|k_{p,e}| = 1.793\ \omega_0/c$) Raman instabilities are attenuated as the ramp time increases from $0.5T_{\rm opt}$ to $10T_{\rm opt}$.

Once the numerical parameters have been set, we look at the possibility of controlling the seed laser amplification by chirping the pump laser field.

IV. CHIRPING THE PUMP LASER FIELD

The backward Raman amplification process results in the energy transfer from the pump beam to the counterpropagating seed pulse through the resonant three-wave coupling with the Langmuir plasma wave. It is then essential that the pump laser beam is not depleted during its propagation along the plasma before reaching the seed pulse and the plasma is not heated too much to optimize the amplification process. Moreover, it is also important to limit the spontaneous Raman scattering that may generate a pedestal pulse preceding the amplified seed beam. Adding a chirp to the pump laser beam appears to be an excellent tool to complete these requirements. It is more simple in practice than producing a plasma density gradient and enables the reduction of the spontaneous Raman growth rate such that $\Gamma^C = \Gamma_0^2/\sqrt{\Gamma_0^2 + (\Delta\omega_p)^2}$, where $\Delta\omega$ is

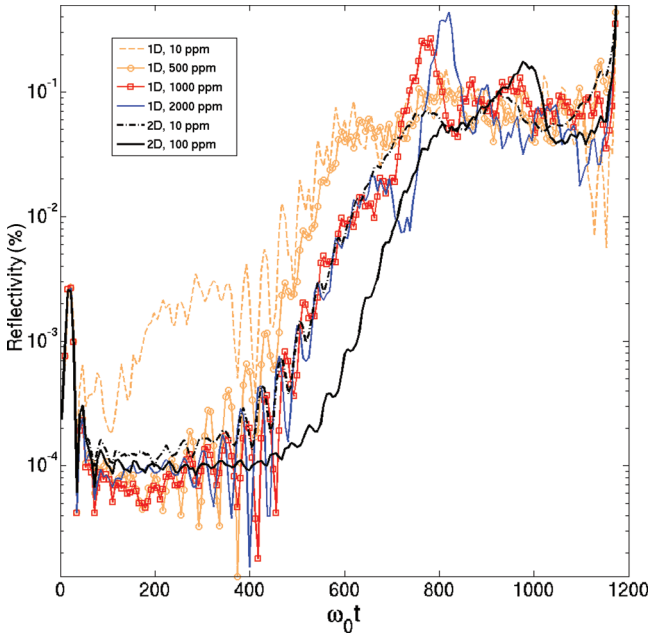

FIG. 5. (Color online) Reflectivity of the pump wave computed in 1D and 2D simulations for different numbers of particles per cell. Here ppm denotes particles per mesh cell.

the pump bandwidth and Γ_0 is the Raman amplification rate for an unchirped pump laser beam [17,18].

The chirp parameter α is defined as

$$\alpha = \frac{1}{\omega_0^2}\frac{\partial \omega(t)}{\partial t}, \tag{15}$$

with $\omega(t)$ the pump instantaneous frequency. The frequency bandwidth of the pump laser beam is then $\Delta\omega_p \approx \alpha\omega_0^2 T_p$, where T_p is the pump pulse duration. The chirp value has to be carefully chosen to optimize the Raman amplification. The phase mismatch between the three waves has to be maintained over the seed pulse propagation. This leads to the condition $\Delta\omega_p \leqslant \Delta\omega_s$, where $\Delta\omega_s$ is the seed frequency bandwidth. The seed temporal pulse in our simulation is chosen to be close to a gate function with a T_s width so that its spectral bandwidth is approximated by $\Delta\omega_s \sim 8/T_s$ and the maximum chirp value is thus limited by $|\alpha| < \frac{8}{(\omega_0 T_s)(\omega_0 T_p)}$. Moreover, the amplification

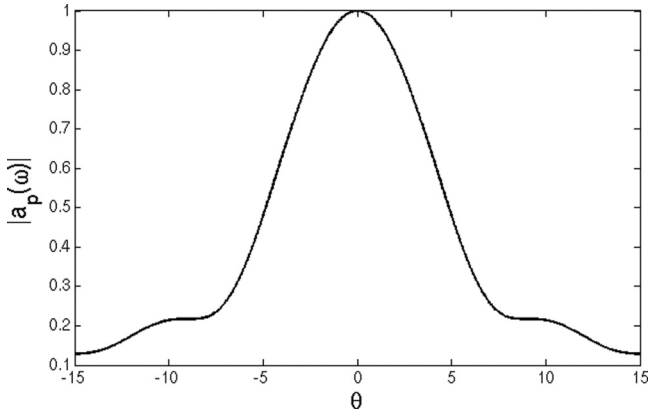

FIG. 6. Spectrum of the linear ramp of the pump laser field [Eq. (12)] with $\theta = (\omega_0 - \omega)\tau$.

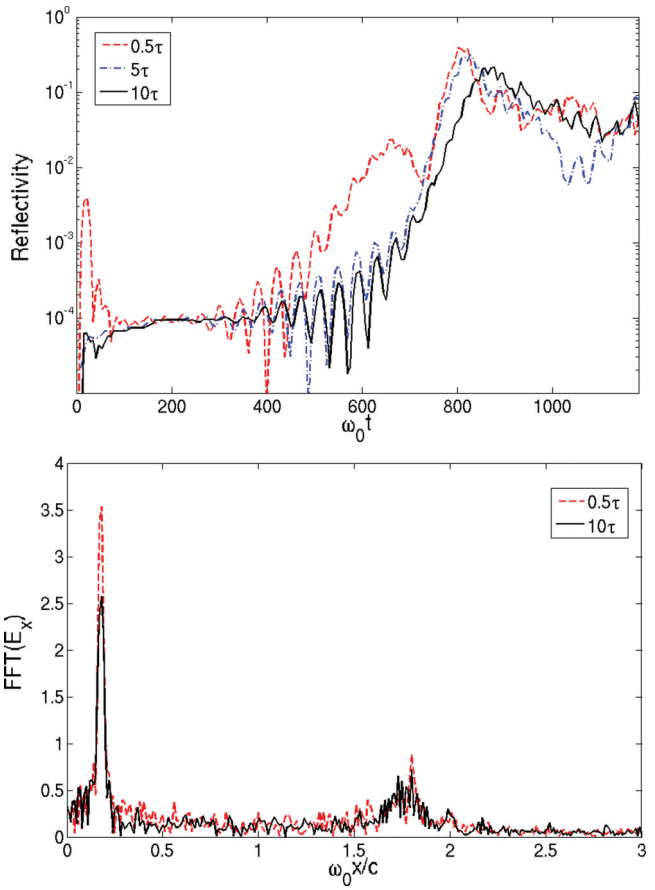

FIG. 7. (Color online) Dependence of the reflectivity on the pump raising time (top) and spatial Fourier spectra of the electrostatic fields (bottom). Here FFT(E_x) denotes the Fourier transform of E_x.

of spontaneous Raman scattering has to be suppressed so that we need $\Delta\omega_p > \Gamma_0$. This results in the minimum chirp value $|\alpha| > \frac{\Gamma_0}{\omega_0^2 T_p}$.

To study the effect of a chirped pump laser beam on the Raman amplification, we have performed 1D and 2D PIC simulations with a numerical box set to 2000 × 800 cells ($80 \times 32\ \mu m^2$). The mesh size is equal to $\Delta x = \Delta y = \lambda_p/20$ (40 nm). The plasma is composed of protons and electrons with an initial zero temperature, occupying the whole box. Its density is equal to $n_0/n_c = 0.03$. The pump and seed laser beams both have amplitudes equal to 0.1. The pump laser beam is characterized by a front rise time over five optical periods followed by a constant amplitude. Its duration is equal to 637 fs. The seed laser pulse amplitude has a $\cos^2$ temporal profile with a width equal to 50 fs. Both laser beams have a $\cos^2$ spatial profile of the amplitude with a width equal to 15.28 μm and centered in 15.3 μm. The seed laser beam is temporally delayed 300 fs. The boundary conditions are absorbing along the longitudinal axis and periodic along the transverse one for both fields and particles. These physical parameters correspond to the optimum chirp values $1.3 \times 10^{-5} \leqslant |\alpha| \leqslant 4.5 \times 10^{-5}$.

We focus our attention on 1D numerical results; here 2000 macroparticles per cell have been set. Figure 8(a) displays the reflectivity computed for different values of the pump laser chirp. Note that we have chosen to display results obtained

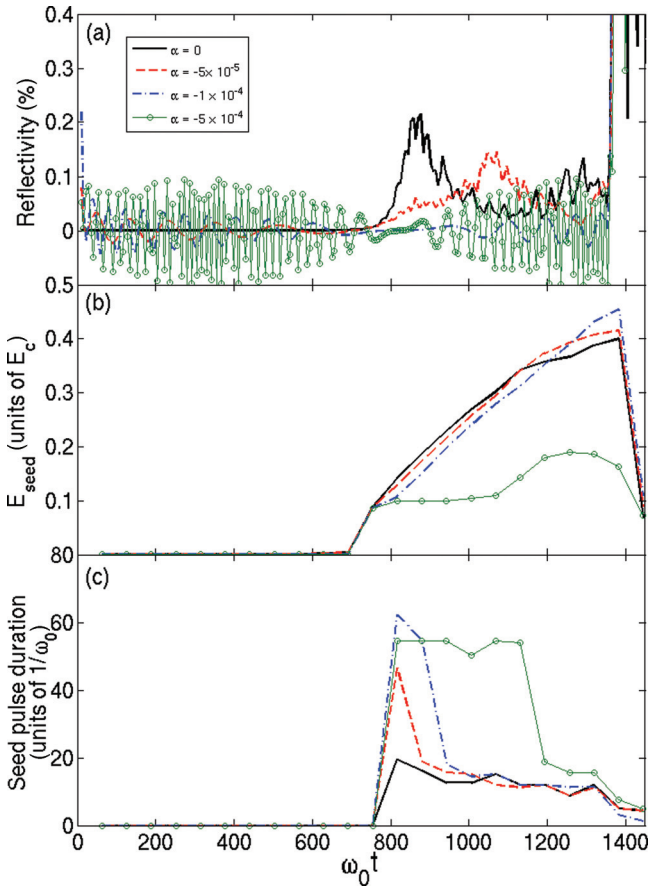

FIG. 8. (Color online) Temporal evolution of (a) the reflectivity, (b) the seed pulse amplitude, and (c) the seed pulse duration for unchirped and chirped pump laser beams. The duration and the energy of the seed laser beam have been set equal to zero for time earlier than $\omega_0 t = 711$ (time at which the seed beam enters the plasma).

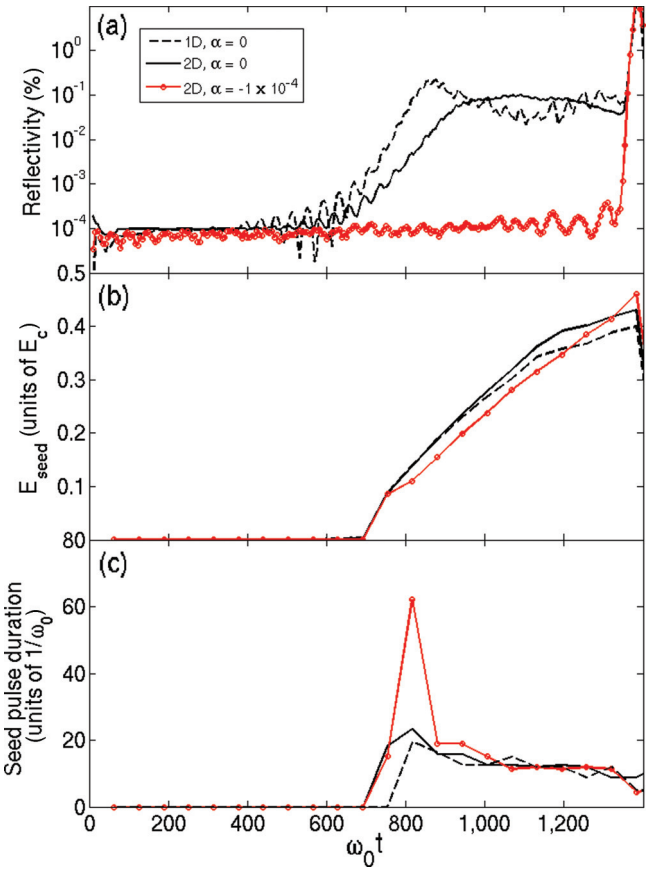

FIG. 9. (Color online) Temporal evolution of (a) the reflectivity, (b) the seed amplitude, and (c) the seed duration for unchirped and chirped pump laser beams in 1D and 2D geometries. The duration and the energy of the seed laser beam have been set equal to zero for time earlier than $\omega_0 t = 711$ (time at which the seed beam enters the plasma). For the 2D geometry, the diagnostics were computed on axis.

with negative chirp values, but identical observation has been made with positive chirp values. The Raman reflectivity is effectively reduced and decreases as the chirp absolute value increases. The reflectivity reduction is optimal for $|\alpha| > 10^{-4}$, which is higher than the theoretical chirp limit ensuring the phase mismatch between the three waves. In fact, this last value has to be increased to 2.6×10^{-4} because we clearly observe in Fig. 8(c) that the seed pulse duration is shortened to 9 fs as it propagates in the plasma. Now considering the amplitude and pulse duration of the seed beam in Figs. 8(b) and 8(c), we note that choosing $|\alpha| = 5 \times 10^{-4}$ makes the amplification less efficient, which is in agreement with a three-wave coupling factor lowering resulting from a phase mismatch. For this configuration, the optimal chirp parameter is then equal to $|\alpha| = 10^{-4}$. It indeed cancels the seed pulse amplitude saturation observed for $\omega_0 t > 1300$ in Fig. 8(b) when the pump laser beam is unchirped. This is in agreement with the theoretical estimates.

These results are confirmed in the two-dimensional simulations in Fig. 9, with 100 macroparticles per mesh. As shown in Fig. 5, the reflectivity computed for unchirped laser beam is reduced in a 2D geometry. We retrieve the previous results, which means a complete suppression of the reflectivity due to the spontaneous Raman scattering and the absence of the saturation in the seed laser beam amplification. The amplification rate is estimated to be 3.5×10^{-4}, which is close to the theoretical estimate $I_p/\tau_s = 5.5\times 10^{-4}$. However, as one can see in Fig. 9(b), before the wavebreaking-induced saturation, the seed laser amplification is less efficient when the pump laser beam is chirped. This is a direct consequence of the spontaneous Raman scattering suppression, which results in a lower plasma wave excitation and thus in a lower pump to seed energy transfer. Figure 9(c) shows the temporal evolution of the seed pulse duration computed on the axis where the pump laser beam is maximal. As observed in 1D simulations, we note a decrease of the pulse duration close to one optical period.

Figure 10 displays the spatial distribution of the seed laser beam amplitude as it enters and leaves the plasma. Along its propagation in the plasma, the seed laser beam undergoes a spatial compression and a temporal shortening resulting from the nonlinear backward Raman amplification. As it reaches the plasma ending, its pulse duration and spatial width are 5 and 2 times lower than the initial values, respectively. We also note an increase of the intensity by a factor 20. The energy transfer rate from the pump beam to the seed laser beam is equal to 2%. Moreover, we note in Fig. 10 that the prepulse is suppressed

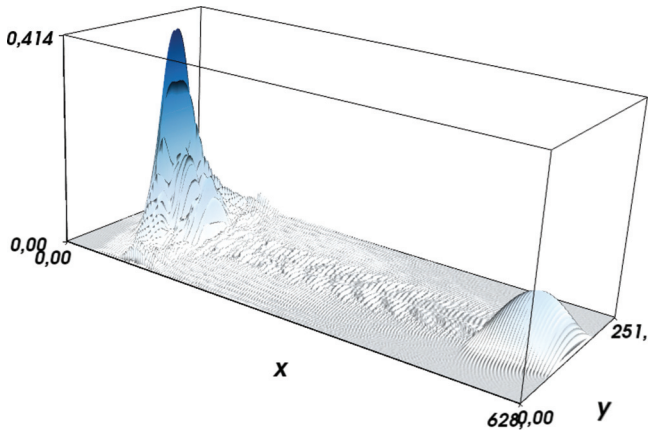

FIG. 10. (Color online) Spatial distribution of the seed laser pulse for two different times as it enters and leaves the plasma. The pump laser beam is chirped ($\alpha = -1 \times 10^{-4}$).

by the chirp and the seed spatial profile is kept smooth and does not undergo any modulational instability.

In weakly collisional plasma, the filamentation instabilities such as the ponderomotive [19] and the relativistic [20] ones can lead the pump laser field to an unstable regime where it undergoes a self-focusing effect and filamentation [18]. It is essential to choose the laser and plasma parameters such that those instabilities could not develop in order to preserve the pump laser spatial distribution and keep the backward Raman amplification efficient. The critical power over which the laser pulse undergoes self-focusing is (in units of MW) $P_{cr} = 34 \times T_e\sqrt{1 - n_e/n_c}/(n_e/n_c)$, (with T_e the electron temperature expressed in keV) for the ponderomotive instability and (in units of GW) $P_{cr} > 16.2/(n_e/n_c)$ for the relativistic one. The associated focal length is $L_{\rm foc} = z_R/\sqrt{P/P_{cr} - 1}$, with z_R the laser Rayleigh length.

In our simulations, the pump laser input power is close to 45 GW, much lower than the critical power for relativistic self-focusing ($P_{cr} = 540$ GW), so that no self-focusing is observed; the electron temperature is initially set to zero. These parameters lead to excellent agreement between numerical results obtained in a 1D geometry and those from two-dimensional simulations. When the plasma density and/or the pump laser power increase, particular attention should be devoted to this instability, which could lead to a deterioration of the backward Raman amplification.

V. CONCLUSION

The backward Raman amplification in linear and nonlinear regimes was studied with a PIC code OCEAN. The numerical simulations performed in a 1D geometry have shown excellent agreement with analytical formulas, thus validating this code. By focusing our attention on the number of particles per cell, we have shown that numerical noise has an important impact on the spontaneous Raman scattering and the backward Raman amplification studies need PIC simulations with a lowered and controlled numerical noise. The PIC simulations performed in 1D and 2D geometries have shown that spontaneous Raman signal can be reduced, and even canceled, by properly chirping the pump laser beam. This makes pump laser chirping a convenient tool to control the prepulse and the pulse shape of the amplified seed laser.

ACKNOWLEDGMENT

The authors are thankful to Emmanuel d'Humières for useful discussions.

[1] G. A. Mourou, N. J. Fisch, V. M. Malkin, Z. Toroker, E. A. Khazanov, A. M. Sergeev, T. Tajima, and B. Le Garrec, Opt. Commun. **285**, 720 (2012).
[2] V. M. Malkin, G. Shvets, and N. J. Fisch, Phys. Rev. Lett. **82**, 4448 (1999).
[3] Y. Ping, I. Geltner, N. J. Fisch, G. Shvets, and S. Suckewer, Phys. Rev. E **62**, R4532 (2000).
[4] W. Cheng, Y. Avitzour, Y. Ping, S. Suckewer, N. J. Fisch, M. S. Hur, and J. S. Wurtele, Phys. Rev. Lett. **94**, 045003 (2005).
[5] Y. Ping, W. Cheng, S. Suckewer, D. S. Clark, and N. J. Fisch, Phys. Rev. Lett. **92**, 175007 (2004).
[6] V. M. Malkin, G. Shvets, and N. J. Fisch, Phys. Rev. Lett. **84**, 1208 (2000).
[7] B. Ersfeld and D. A. Jaroszynski, Phys. Rev. Lett. **95**, 165002 (2005).
[8] G. Vieux, A. Lyachev, X. Yang, B. Ersfeld, J. P. Farmer, E. Brunetti, R. C. Issac, G. Raj, G. H. Welsh, S. M. Wiggins, and D. A. Jaroszynski, New J. Phys. **13**, 063042 (2011).
[9] J. A. Caird, IEEE J. Quantum Electron. **QE-16**, 489 (1980).
[10] R. M. G. M. Trines, F. Fiúza, R. Bingham, R. A. Fonseca, L. O. Silva, R. A. Cairns, and P. A. Norreys, Nat. Phys. **7**, 87 (2010).
[11] R. M. G. M. Trines, F. Fiúza, R. Bingham, R. A. Fonseca, L. O. Silva, R. A. Cairns, and P. A. Norreys, Phys. Rev. Lett. **107**, 105002 (2011).
[12] G. L. Lamb, Jr., Rev. Mod. Phys. **43**, 99 (1971).
[13] N. A. Yampolsky, V. M. Malkin, and N. J. Fisch, Phys. Rev. E **69**, 036401 (2004).
[14] C. K. Birdsall and A. B. Langdon, *Plasma Physics via Computer Simulation* (Tayler & Francis, London, 2005).
[15] Y. Sentoku and A. Kemp, J. Comput. Phys. **227**, 6846 (2008).
[16] T. Zh. Esirkepov, Comput. Phys. Commun. **135**, 144 (2001).
[17] W. L. Kruer, *The Physics of Laser Plasma Interactions* (Westview, Boulder, 2003).
[18] D. Pesme, *La Fusion Thermonucléaire Inertielle par Laser* (Eyrolles, Paris, 1993).
[19] P. Kaw, G. Schmidt, and T. Wilcox, Phys. Fluids **16**, 1522 (1973).
[20] G.-Z. Sun, E. Ott, Y. C. Lee, and P. Guzdar, Phys. Fluids **30**, 526 (1987).